Charge correlations and isotopic distributions of projectile fragmentation events in ^{124}Xe + ^{112}Sn at $E/A = 50$ MeV

S. Hudan,* A. B. McIntosh, J. Black, D. Mercier, C. J. Metelko,† R. Yanez,‡ and R. T. de Souza
Department of Chemistry and Indiana University Cyclotron Facility, 2401 Milo B. Sampson Lane, Bloomington, Indiana 47405, USA

A. Chbihi
GANIL, Caen, France

M. Famiano
Western Michigan University, Kalamazoo, Michigan, USA

M. O. Frégeau, J. Gauthier, J. Moisan, and R. Roy
Université Laval, Québec, Canada

S. Bianchin, C. Schwarz, and W. Trautmann
GSI Helmholtzzentrum GmbH, Planckstrasse 1, D-64291 Darmstadt, Germany

A. S. Botvina
Institute for Nuclear Research, Russian Academy of Sciences, RU-117312 Moscow, Russia
(Received 6 October 2009; published 29 December 2009)

Ternary breakup of an excited projectile-like fragment produced in mid-peripheral collisions of ^{124}Xe projectiles with ^{112}Sn nuclei at $E/A = 50$ MeV is examined. Charge correlations reveal that symmetric breakups occur with significant probability. By selecting on the parallel velocity of the heaviest fragment we minimize the entrance channel dynamics. Calculations with the statistical decay code GEMINI failed to reproduce the experimental charge correlations for any suitable combination of excitation energy and spin considered. A statistical multifragmentation model (SMM) in which breakup of low-density nuclear matter is assumed was able to reproduce the observed charge correlations. The $\langle N \rangle / Z$ and isotope distributions of fragments were compared to the results of the SMM calculations. Describing the $\langle N \rangle / Z$ of heavy fragments ($Z > 6$) within SMM suggests that a reduction of the symmetry energy parameter from $\gamma = 25$ to 14 MeV is necessary. We observe that the yield of neutron-rich isotopes of heavy fragments is particularly sensitive to the symmetry energy.

DOI: 10.1103/PhysRevC.80.064611 PACS number(s): 21.65.Ef, 25.70.Mn

I. INTRODUCTION

The density dependence of the symmetry energy in the nuclear equation of state is a quantity of significant interest [1–8]. It is important in a variety of environments ranging from the crusts of neutron stars to supernovae where the binding of neutron-rich nuclei impacts the nucleosynthetic *r*-process path. In the case of neutron star crusts, the nuclear symmetry energy strongly influences what phases exist within the star and their stability [6]. The composition of the inner crust [6], the nature of crustal vibrations [9], and the star radius [10] are all impacted by the magnitude and density dependence of the symmetry energy. In the laboratory, different experimental approaches have attempted to probe the density dependence of the symmetry energy. Among these varied approaches are examining the transport of neutrons and protons between colliding nuclei at intermediate energies [7] and measuring the neutron skin thickness in ^{208}Pb [11].

A significant issue confronts the extraction of information on the symmetry energy from intermediate-energy heavy-ion reactions. Such reactions, particularly for mid-peripheral collisions, manifest a strong influence of the collision dynamics [12–15]. The extent to which this collision dynamics influences the isotopic composition of the measured particle yields and the nucleon transport is presently unclear. To minimize this impact, in recent studies the ratios of reactions have been constructed in such a way that the fragment yield ratios are examined, so as to mitigate the impact of the reaction dynamics [3,7]. This double-ratio approach should cancel the influence of the reaction dynamics to first order. In the present work we follow an alternate approach. We select a reaction channel for which the role of the reaction dynamics is minimized and the statistical decay properties are dominant. Specifically, we elect to investigate the ternary decay of an excited projectile-like fragment, PLF*.

*shudan@indiana.edu
†Present address: Particle Physics Department, Rutherford Appelton Laboratories, Didcot, UK.
‡Present address: Department of Chemistry, Oregon State University, Corvallis, Oregon, 97331, USA.

II. EXPERIMENTAL SETUP

The experiment was conducted at the GANIL facility in Caen, France, where beams of ^{112,124}Xe ions accelerated to $E/A = 50$ MeV impinged on ^{112,124}Sn targets with a typical beam intensity of $\approx 10^8$ particle/s. Charged products of the reaction were identified by two detector arrays located within a thin-wall aluminum scattering chamber. One array, FIRST [16], consisting of annular segmented silicon detectors backed by CsI(Tl) crystals with photodiode readout, subtended the angular range $3^\circ \leqslant \theta_{\rm lab} \leqslant 14^\circ$. The most forward telescope in FIRST, $3^\circ \leqslant \theta_{\rm lab} \leqslant 7^\circ$, provided the identification by atomic number of all products up to $Z = 55$ and additionally allowed isotopic information for $Z \leqslant 14$. This telescope in FIRST, designated T1, consisted of a Si(IP)-Si(IP)-CsI(Tl)/PD stack in which the silicon detectors were 270 and 980 μm thick. Both silicon detectors in T1 had 48 concentric rings on the junction side and 16 pie-shaped sectors on the ohmic side (S2 design) [17]. The larger angle telescope in FIRST was a Si(IP)-CsI(Tl) stack with a 500-μm-thick silicon S1 design detector [17] as the first element. This detector has 16 rings, further subdivided into four quadrants on the junction side, along with 16 pie-shaped sectors on the ohmic surface. Each CsI(Tl) crystal in T1 and T2 matched the pie-shaped geometry of the silicon in front of it. The high segmentation of FIRST provided an angular resolution of $\pm 0.045^\circ$ ($3^\circ \leqslant \theta_{\rm lab} \leqslant 7^\circ$) and $\pm 0.23^\circ$ ($7^\circ \leqslant \theta_{\rm lab} \leqslant 14^\circ$) in polar angle and $\pm 11.25^\circ$ in azimuthal angle. The numerous detector segments were processed with multiplexed analog shaping electronics (MASE) [18]. The obtained energy resolution of 0.5% was characteristic of this type of detector. Charged particles emitted at larger laboratory angles were identified in the LASSA array [19], which provided isotopic identification of fragments for $Z \leqslant 8$. This charged particle experimental setup provided good characterization of fragments forward of the center of mass. All our subsequent analysis is therefore restricted to fragments emitted forward of the center of mass. Neutrons emitted in this experiment were identified by 27 detectors of the DEMON array [20]; however, the neutron data are not utilized in the present analysis.

III. EXPERIMENTAL RESULTS

In this work we focus on the fragmentation of the PLF* for the system ^{124}Xe + ^{112}Sn at $E/A = 50$ MeV. We begin by examining the correlation between the multiplicity of $Z \geqslant 3$ fragments and the size of the fragments. In Fig. 1, for a given atomic number of the heaviest fragment (Z_H) and a given multiplicity, the average charge of all fragments excluding the heaviest fragment is displayed. When $M(Z \geqslant 3) = 2$, the Z_H distribution is broad and extends from $Z_H = 4$ to $Z_H = 52$. Associated with heavy fragments with $12 \leqslant Z_H \leqslant 35$, the average atomic number of the second fragment is approximately 7.5. When $M(Z \geqslant 3) = 3$, an average fragment atomic number of $Z \approx 7$ is associated with $15 \leqslant Z_H \leqslant 18$. The total charge associated with the three fragments is ≈ 30, a large fraction of the atomic number of the projectile. Events in which multiple fragments have a sum charge corresponding to a large fraction of the projectile atomic number and which

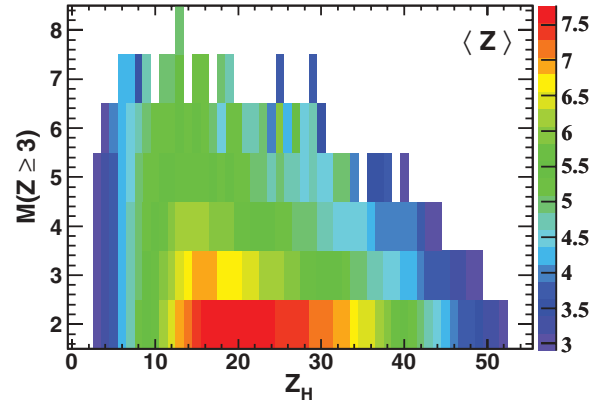

FIG. 1. (Color online) Correlation between the multiplicity of fragments with $Z \geqslant 3$ and the atomic number of the heaviest measured fragment. The color scale indicates the average fragment size excluding the heaviest fragment.

may be associated with the fragmentation of the projectile are also observed for $M = 4$ events.

To ascertain the kinematic regime populated by these fragments we examine the parallel velocity distributions for the different fragments in ternary events in Fig. 2. As expected, the heaviest fragment, Z_H, exhibits a peaked distribution damped from the beam velocity (which is indicated by a dotted line). Previous work has related the velocity damping of the projectile to its excitation [21]. In contrast, the parallel velocity distributions for $4 \leqslant Z \leqslant 5$ fragments and $10 \leqslant Z \leqslant 12$ fragments are broad. The distribution for $4 \leqslant Z \leqslant 5$ has a bimodal nature with the majority of the yield associated with $7 \leqslant v_\parallel \leqslant 10$ cm/ns. These fragments are likely not associated with mid-velocity emission but rather represent projectile breakup events. In the case of $10 \leqslant Z \leqslant 12$ fragments, a slightly narrower distribution is observed with the bulk of the yield also associated with the kinematic regime of the PLF*.

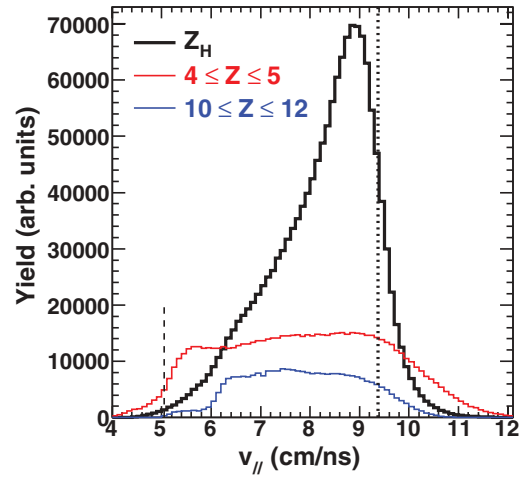

FIG. 2. (Color online) Parallel velocity in the laboratory frame for fragments associated with ternary events ($Z \geqslant 3$). The distributions for Z_H and different ranges in atomic number are displayed. The dashed line indicates the center-of-mass velocity; the dotted line corresponds to the beam velocity.

We subsequently focus on events in which at least three charged products detected in the angular range $3^\circ \leqslant \theta_{\rm lab} \leqslant 14^\circ$ were selected. In addition, to ensure that a large fraction of the original projectile-like fragment was detected, we required that a minimum total charge of $\sum Z \geqslant 27$ was measured in FIRST. For events selected in this mode, the detected charged products are sorted on the basis of atomic number, with the largest atomic number ("heaviest") referred to as Z_H, the second largest ("medium") as Z_M, and the third largest ("lightest") as Z_L.

A. Experimental charge correlation

We begin by investigating the correlation between the atomic number of the three largest products. This correlation is presented in the symmetrized charge-Dalitz representation [22,23] in Fig. 3, where each ternary event is represented by a single point. For all fragments included in the diagram the minimum atomic number for a fragment is $Z = 2$. In this Dalitz diagram, the distances to the sides correspond to the values $Z_H/Z_{\rm TOT}$, $Z_M/Z_{\rm TOT}$, and $Z_L/Z_{\rm TOT}$, where $Z_{\rm TOT} = Z_H + Z_M + Z_L$. Events with a large fragment and two small particles populate the corners of the triangle, whereas events with symmetric charge sharing populate the center of the triangle. Clearly evident in Fig. 3 is a large yield in the corners of the diagram. This yield corresponds to the detection of a heavy fragment in coincidence with two $Z = 2$ particles—which are most likely α particles. This charge correlation pattern is hardly surprising as peripheral collisions will lead to a slightly excited projectile-like fragment. This PLF* will decay principally by evaporating nucleons and light charged particles (n, $Z = 1$, and $Z = 2$). From the corners of the triangle one also observes a ridge of yield oriented along each side of the triangle. Such events can be thought of as emission of an intermediate-mass fragment (IMF: $Z \geqslant 3$) together with the emission of a light charged particle (LCP). Emission of IMFs from the PLF* produced in mid-peripheral collisions has been observed at moderate excitation energy, $E^*/A \simeq 4$ MeV [21]. Events located closer to the midpoint of a side of the Dalitz triangle are associated with more equal-sized Z_H and Z_M. In addition to the yield in the corners and the yield along the sides of the Dalitz diagram, there is a broad, relatively uniform distribution of yield throughout the Dalitz diagram. This broad distribution corresponds to relatively equiprobable charge partitions.

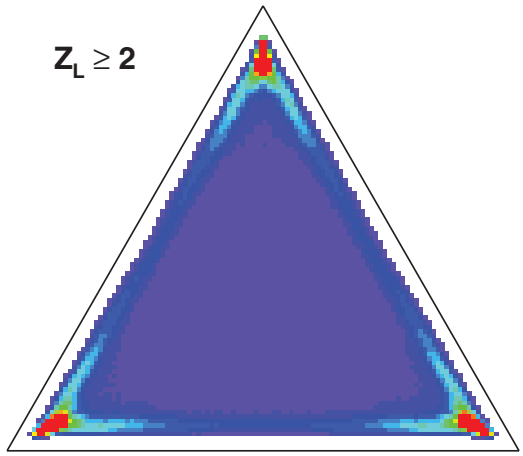

FIG. 3. (Color online) Dalitz diagram for events with at least three charged particles in the angular range $3^\circ \leqslant \theta_{\rm lab} \leqslant 14^\circ$ for the system ^{124}Xe + ^{112}Sn at $E/A = 50$ MeV. A minimum Z of 2 is required for the third-largest product. The color scale is linear.

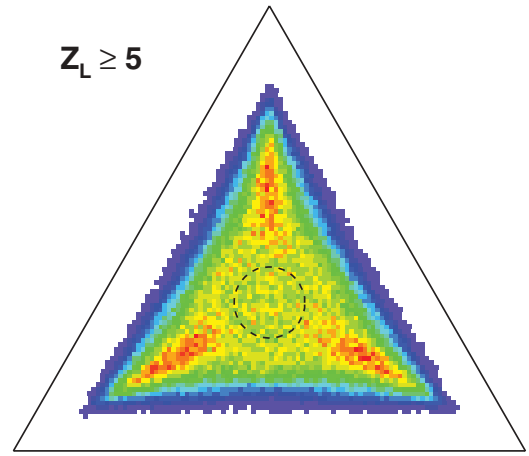

FIG. 4. (Color online) Similar to Fig. 3 with a minimum Z of 5 for the third-largest fragment. The dashed line corresponds to a circle of radius $R_{\rm sym} = 0.08$ centered on the center of the triangle.

To suppress events corresponding to the emission of two light charged particles (or light IMFs) from a modestly excited PLF*, we imposed the restriction that $Z_L \geqslant 5$. The resulting charge correlation between the three fragments is shown in Fig. 4. These events represent ≈15% of the ternary events shown in Fig. 3. The requirement on the minimum atomic number of Z_L eliminates yield along the edges of the Dalitz triangle. It is clearly evident that the charge correlation pattern observed in Fig. 4 differs significantly from that observed in Fig. 3. With the requirement that $Z_L \geqslant 5$, the dominant yield is present along a line connecting each vertex with the center of the triangle. As one moves from the vertex toward the center, the yield first increases, reaches a maximum, and then decreases. This yield is associated with one larger fragment in coincidence with two smaller fragments of comparable size. It is interesting to note that this yield is larger than that associated with one smaller fragment ($Z_L \approx 5$) and two equal size larger fragments. In addition, one also observes yield located at the center of the triangle corresponding to the detection of three fragments of approximately equal size.

To examine this tripartition into equal sized fragment in more detail, we selected events associated with the center of the triangle, as indicated by the dashed line in Fig. 4. This circle has a radius of $R_{\rm sym} = 0.08$ or 12% of the distance to the nearest apex of the triangle. For events in this circle, the average $\Delta Z = Z_H - Z_L$ has a value of 2.6. Essentially all the yield (>95%) has a $\Delta Z \leqslant 4$. These events selected in the center of the Dalitz diagram correspond to ≈10% of the events with a multiplicity of three and above and $Z_L \geqslant 5$.

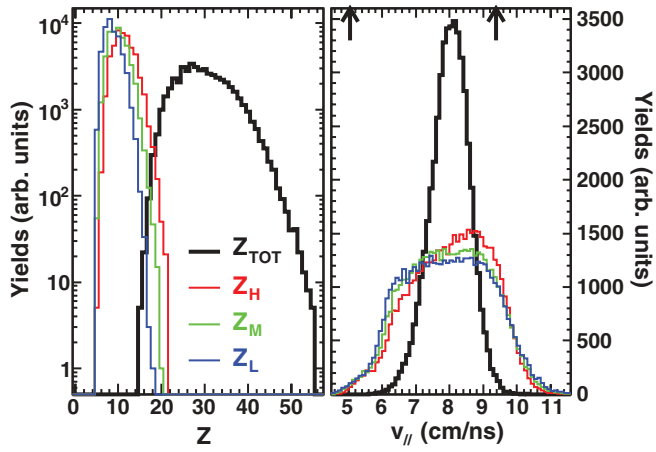

FIG. 5. (Color online) Left: Atomic number for Z_H (red), Z_M (green), and Z_L (blue), selected in the center of the Dalitz diagram. The thick black line corresponds to Z_{TOT}. Right: Parallel velocity in the laboratory frame for Z_H, Z_M, Z_L, and the center of mass of the three fragments (thick black line).

B. Properties of symmetric events

In the subsequent analysis, we select events with a $Z_L \geqslant 5$, which populate the center of the Dalitz diagram, as indicated by the dashed circle. We refer to these events as symmetric breakup events. Distributions of the atomic number and parallel velocity in the laboratory frame for the three biggest fragments are displayed in Fig. 5. Based on our selection of events near the center of the Dalitz diagram, the atomic number distributions of the three biggest fragments should be similar. Indeed, as shown on the left panel of Fig. 5, the atomic numbers of the three fragments largely overlap. A slight hierarchy in size, however, can be observed. The average Z_H, Z_M, and Z_L are 11.35, 10.03, and 8.71, respectively. The Z_{TOT} distribution covers a broad range from $Z_{\mathrm{TOT}} = 15$ (determined by the minimum Z requirement of $Z = 5$) to the atomic number of the projectile ($Z = 54$). The average size of the system composed of the three biggest fragments is $\langle Z_{\mathrm{TOT}} \rangle = 30.09$, corresponding to ≈56% of the projectile. The granularity and geometric coverage of our experimental setup allow measurement of light particles and fragments in coincidence with the three selected fragments. For these events, the average charge measured at forward angles is ≈34, accounting for ≈63% of the projectile reflecting the mid-peripheral nature of the collision. Hence, these three largest fragments contain ≈90% of the total charge observed in this angular range $3^\circ \leqslant \theta_{\mathrm{lab}} \leqslant 14^\circ$. The parallel velocity distributions of these three fragments, in the laboratory frame, are shown in the right panel of Fig. 5. All three individual distributions are broad, ranging from 5.5 to 10.5 cm/ns. For reference, the projectile and center-of-mass system velocities, indicated by the arrows, are 9.38 and 5.05 cm/ns, respectively. These velocity distributions indicate that the three fragments do *not* originate from mid-rapidity but have velocity distributions centered at 8 cm/ns. This large velocity is suggestive of a dissipative binary collision in which the excited PLF* created subsequently decays. Although the second and third biggest fragments exhibit similar velocity distributions, the biggest fragment distribution is slightly narrower and somewhat more asymmetric, with a most probable velocity of ≈8.5 cm/ns. We have constructed the velocity distribution of the center of mass of the three fragments. The resulting velocity is displayed as the thick solid black line in Fig. 5. The peak of the center-of-mass velocity distribution is situated at ≈8 cm/ns. If one assumes that these three fragments originate from the PLF*, their center-of-mass velocity reflects the velocity damping incurred, namely ≈1.4 cm/ns from the projectile velocity. For a similar system at the same incident energy in which reconstruction of the PLF* was performed, this velocity damping was deduced to be related to an average excitation energy of ≈4–5 MeV/A [21]. Also notable is that the center-of-mass velocity distribution is considerably narrower than the velocity distributions of the individual three fragments. The center-of-mass velocity distribution has a width (second moment) of $\sigma \approx 0.6$ cm/ns as compared to widths of ≈1.2 cm/ns for the individual fragments. The difference in the widths of the individual fragment and the center-of-mass distributions is due to momentum conservation.

The atomic number and velocity distributions of the three biggest fragments reveal that we have selected collisions in which on average a relatively large PLF* (≈60% of the projectile) is produced. This PLF* has an average velocity damped ≈1.4 cm/ns from the beam velocity and subsequently undergoes decay into at least three fragments. The events selected in this fashion contrast markedly with aligned decay of an excited projectile-like fragment in which a strong correlation between the magnitude of the fragment velocities and the atomic number of the fragments was observed [14]. For the presently selected events, only a slight correlation between the size (atomic number) and velocity of the fragments is observed. Nevertheless, the largest fragment has a slightly higher velocity on average than the other two fragments, indicating a slight memory of the entrance channel.

To explore this memory of the entrance channel further, we examined momentum correlations between the three fragments. For events populating the center of the Dalitz diagram we examine the momenta between the three fragments. The quantities P_{H-L} and P_{H-M} correspond to the relative momenta between the heavy and light or heavy and medium fragments respectively. In constructing the momentum of each fragment, we utilized the experimentally measured mass number for $3^\circ \leqslant \theta_{\mathrm{lab}} \leqslant 7^\circ$ and $Z \leqslant 14$. For fragments in the range $7^\circ \leqslant \theta_{\mathrm{lab}} \leqslant 14^\circ$ or $Z \geqslant 14$ we utilized the evaporator attractor line systematics [24]. Using the mixed event technique [25] we then constructed a "background" by selecting three fragments from three different events. These fragments populate the same overall phase space as the fragments within an event and are subject to the same kinematical acceptances but lack any correlation existing between fragments within an event. Shown in the top two panels of Fig. 6 are the ratio of the correlated and uncorrelated momentum distributions. Both distributions manifest a suppression of relative yield at low relative momentum. The relative suppression of correlated yield for low relative momenta is indicative of the

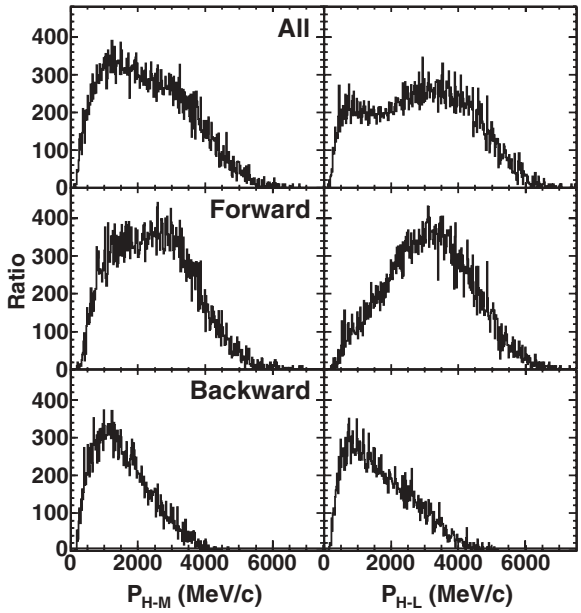

FIG. 6. One-dimensional projections of the two-dimensional correlation function between the heavy-light and heavy-medium fragments. See text for details.

Coulomb repulsion between the fragments. The most notable feature of these distributions is the peak centered at $P_{H-L} = 3500$ MeV/c. It should also be noted that a slight shoulder exists in P_{H-M} at approximately the same momentum. Examination of the events populating this peak (and shoulder) reveals that they are associated with the preferential orientation of the heavy fragment at higher parallel velocity than the medium fragment. This correlation between the fragment size and velocity is a distinct feature of the decay of an elongated projectile-like fragment produced in a dissipative mid-peripheral collision and is a clear indication of the persistence of the entrance channel dynamics [14,26]. To suppress the contribution of such dynamical decays, we further subdivided the events based on the parallel velocity of the fragments relative to the center of mass of the three fragments. Events in which $V_H > V_{\rm CM}$ we designate as "forward" and those in which $V_H < V_{\rm CM}$ we designate as "backward." The ratios corresponding to the "forward" and "backward" cases are shown in the middle and lower rows of Fig. 6. These distributions demonstrate that the peak observed at $P_{H-L} = 3500$ MeV/c is clearly associated with configurations in which the heavy fragment has a higher parallel velocity than the center of mass of the three fragments. In contrast, requirement that $V_H < V_{\rm CM}$ (i.e., the heavy fragment is "backward") dramatically suppresses the relative yield for $P_{H-M} > 2000$ MeV/c. As selection of the "backward" emission case suppresses the dynamical correlations associated with the entrance channel, we subsequently focus on these events where the statistical nature of the projectile-like fragment decay is dominant. In the subsequent analysis, we refer to events in which three large fragments of similar size are observed in the final state as ternary breakup events.

IV. COMPARISON TO STATISTICAL MODELS

Dynamical models used for description of the initial stage of the reaction lead to the conclusion that after a time interval of few tens of fm/c, when fast particles have left the system, the character of the process in the remaining nuclear residues changes. Owing to the large degree of nucleon-nucleon scattering, the system rapidly approaches equilibrium and manifests equilibrium features. This quasi-equilibrated system subsequently undergoes statistical decay. Consequently, we compare the pattern of the experimentally observed charge correlations with the predictions of two different statistical models describing the statistical decay of the PLF*. The code GEMINI utilizes a transition state formalism to describe the sequential decay of an excited nucleus [27,28]. This model has been successfully used to describe the evaporation of light charged particles and clusters from a heavy excited nucleus, fission [27,29,30], and spallation reactions [31]. In contrast, in the statistical multifragmentation model (SMM) statistical equilibrium between fragments and nucleons in a low-density freeze-out volume is assumed [32,33].

A. Comparison to GEMINI

The statistical model code GEMINI [27,28] employs a Hauser-Feshbach formalism to describe the statistical emission of particles from a compound nucleus of (Z, A) characterized by an excitation energy E^* and spin J. The model follows the decay of the compound nucleus through a series of sequential binary decays. We investigate whether the symmetric ternary breakup observed experimentally can be described within this approach. To account for particles and fragments emitted in coincidence with the three biggest fragments ($\langle Z_{\rm TOT}\rangle = 30.08$), calculations were performed for a nucleus with $Z = 45$ and $A = 103$. The mass of the system was chosen to match the N/Z ratio of the ^{124}Xe projectile, $N/Z = 1.3$. The decay of the nucleus was calculated for excitation energies of 4 and 5 MeV/A and spin between $0\hbar$ and $42\hbar$. The corresponding Dalitz diagrams are displayed in Fig. 7. In construction of the Dalitz diagrams, no restriction was placed on Z_L to depict the full characteristics of the model calculations. For an excitation energy of 4 MeV/A and a spin of $0\hbar$, the large majority of the simulated events lie in the corner of the Dalitz diagram, corresponding to a large residue, $\langle Z_H\rangle \approx 32.6$, and two light charged particles, $\langle Z_M\rangle \approx 2.8$ and $\langle Z_L\rangle \approx 1.7$. The sides of the triangles are slightly populated, <4% of the total yield, indicating decay by fission. The lack of yield in the center of the Dalitz plot demonstrates that for this excitation energy and spin, GEMINI does not produce symmetric ternary breakup of the nucleus into three large fragments. With increasing spin (top right panel of Fig. 7), the fission probability increases, corresponding to ≈19% of the total yield. With increasing excitation energy, $E^*/A = 5$ MeV, the fission probability increases slightly to ≈7% and ≈20% for spins of $0\hbar$ and $42\hbar$, respectively. One also observes the appearance of a small branch originating from the corners of the triangle and oriented toward the center, corresponding to a big fragment coincident with two smaller fragments of approximately the same size. The highest probability for symmetric ternary breakup is

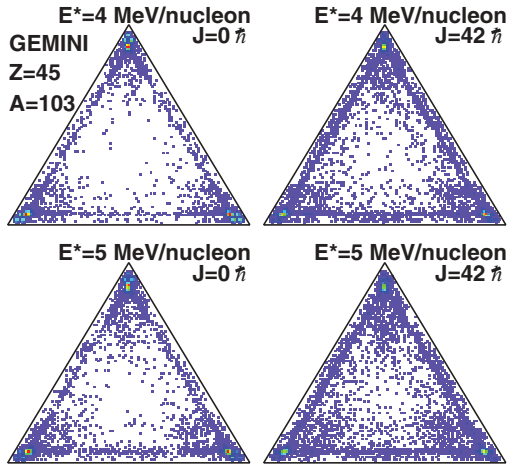

FIG. 7. (Color online) Dalitz diagrams calculated by GEMINI [27,28] for a compound nucleus with $Z = 45$, $A = 103$. Excitation energy and spin of the compound nucleus are indicated on the figure. Events with at least three charged particles and a minimum Z of 1 for the third-largest product are displayed. The diagrams have been normalized and are displayed with the same linear color scale.

reached for the highest excitation energy and spin shown, $E^*/A = 5$ MeV and $J = 42\hbar$, and is of the order of 0.1%.

From examination of Fig. 7, one concludes that, within the statistical code GEMINI, a system with $A \approx 100$, $E^*/A =$ 4–5 MeV, and low or modest spin does not undergo symmetric ternary breakup. Although the introduction of angular momentum increases the probability of decay by the fission channel, it does not result in any significant probability of a symmetric ternary breakup final state. Expansion of a mononucleus in response to thermal pressure has been shown to significantly enhance surface fragment emission [34–36]. The presented experimental data provide a potentially useful benchmark for comparison with such models.

B. Comparison to the SMM

We have also compared the experimental symmetric ternary breakup to the results of the SMM. This model is based upon the assumption of statistical equilibrium between produced fragments in a low-density freeze-out volume [32]. All breakup channels (partitions) composed of nucleons and excited fragments are considered, and the conservation of mass, charge, momentum, and energy is taken into account. An advantage of the model is that the formation of a compound nucleus is included as one of the channels. This allows for a smooth transition from decays via evaporation and fission at low excitation energies [37] to the multifragmentation at high excitation. In the microcanonical treatment the statistical weight of the decay channel j is given by $W_j \propto \exp S_j$, where S_j is the entropy of the system in channel j, which is a function of the excitation energy E^*, mass number A_0, charge Z_0, and other parameters of the source. After the system breakup in the freeze-out volume, the fragments propagate independently in their mutual Coulomb field and undergo secondary decays. The deexcitation of the hot primary fragments proceeds via evaporation, fission, or Fermi breakup [38].

In the SMM calculations, light fragments with mass number $A \leqslant 4$ are considered as stable particles (nuclear gas) with masses and spins taken from the nuclear tables. Only translational degrees of freedom of these particles contribute to the entropy of the system. Fragments with $A > 4$ are treated as heated nuclear liquid drops, and their individual free energies F_{AZ} are parametrized as a sum of the bulk, surface, Coulomb, and symmetry energy contributions:

$$F_{AZ} = F^B_{AZ} + F^S_{AZ} + E^C_{AZ} + E^{\rm sym}_{AZ}. \quad (1)$$

In this standard expression $F^B_{AZ} = (-W_0 - T^2/\epsilon_0)A$ is the bulk energy term, where the parameter ϵ_0 is related to the level density, and $W_0 = 16$ MeV is the binding energy of infinite nuclear matter; $F^S_{AZ} = B_0 A^{2/3}(\frac{T_c^2 - T^2}{T_c^2 + T^2})^{5/4}$ is the surface energy term, where $B_0 = 18$ MeV is the surface coefficient, and $T_c = 18$ MeV is the critical temperature of infinite nuclear matter; $E^{\rm sym}_{AZ} = \gamma(A - 2Z)^2/A$ is the symmetry energy term, where $\gamma = 25$ MeV is the symmetry energy parameter. These parameters are those of the Bethe-Weizsäcker formula and correspond to the assumption of isolated fragments with normal density in the freeze-out configuration, an assumption found to be quite successful in many applications. However, in a more realistic treatment primary fragments in the freeze-out volume should be considered with modifications as a result of a residual nuclear interaction between them. These effects can be accounted for in the fragment free energies by changing the corresponding liquid-drop parameters, if they are indicated by the experimental data. The Coulomb energy may be obtained in the Wigner-Seitz approximation: $E^C_{AZ} = cZ^2/A^{1/3}$, where c is the parameter $c = (3/5)(e^2/r_0)[1 - (\rho/\rho_0)^{1/3}]$, with the charge unit e and $r_0 = 1.17$ fm. However, in the Markov chain SMM used in this paper we can directly calculate the Coulomb interaction of fragments by taking into account their positions in the freeze-out volume.

The new version of SMM [33] is based on generating a Markov chain of partitions that is representative of the whole partition ensemble. Individual partitions are generated and selected into the chain by applying the Metropolis algorithm and taking into account that fragments with the same mass A and charge Z are indistinguishable. Owing to the high efficiency of this method, one can directly calculate the Coulomb interaction energy for each spatial configuration of primary fragments at breakup. One can also calculate the moments of inertia for individual configurations and take into account angular momentum conservation. In this way, one can take into account the correlations between the primary fragment positions and their Coulomb and rotation energies that influence the partition probabilities. The new version is consistent with the previous one based on the Wigner–Seitz approximation: For an isolated thermal source the mean parameters of produced fragments obtained in the standard and the Markov chain versions fit each other reasonably well [33]. We believe that for relatively small systems the Markov-chain SMM is a better choice for analysis of the nuclear multifragmentation data concerning the isospin degree of freedom, when angular momentum may be important.

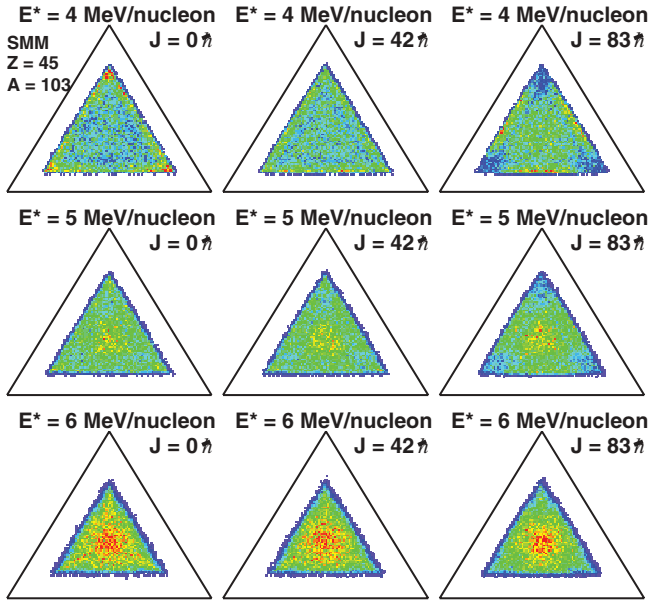

FIG. 8. (Color online) Dalitz diagrams calculated by the SMM [32] for a system with $Z = 45$, $A = 103$. Excitation energy and spin of the system are indicated on the figure. Events with at least three charged particles and a minimum Z_L of 5 are displayed. The diagrams have been normalized and are displayed with the same linear color scale.

In the calculations we have also included a new version of the secondary decay of primary fragments, which takes into account possible modifications of their properties, in particular the reduction of their symmetry energy, in a hot, freeze-out environment as described in Ref. [39].

Calculations were performed for a system with $Z = 45$ and $A = 103$ and different values of excitation energy and spin. The system spin was taken as $J = 0\hbar$, $42\hbar$, and $83\hbar$ and the excitation energy was varied between 4 and 6 MeV/A. The resulting Dalitz diagrams, for a minimum Z_L of 5, are shown in Fig. 8 for all combinations of excitation energy and spin. For an excitation energy of 4 MeV/A and no spin (top left panel on Fig. 8), the majority of the events lie in the corner of the triangle. A big "residue" in coincidence with two fragments with $Z = 5$ (the minimum Z requirement) is characteristics of these events. With increasing spin, the population of the side of the Dalitz diagram increases, indicating an increase in the fission probability. With an extreme spin of $J = 83\hbar$, symmetric ternary breakup, selected on the center of the triangle, occurs with a probability of 9.5%. This probability corresponds to a slight increase when compared to the calculation at the same excitation energy and no spin (7%). Although the probability for events in the center of the Dalitz diagram is roughly comparable to the experimentally observed probability of 10%, the SMM calculation with $E^*/A = 4$ MeV and $83\hbar$ does not exhibit the same overall charge correlation pattern as the experimental data (see Fig. 4). The SMM calculation manifests a much larger fission probability. For an excitation energy of 5 MeV/A (the second row of Fig. 8), the population of symmetric ternary breakups increases with a probability ranging from 12.2% for a spin of $0\hbar$ to 12.9% for $83\hbar$. Although the observed patterns for spins of $0\hbar$ and $42\hbar$ are similar, a spin of $83\hbar$ induces a depletion of evaporation-like events in favor of fission-like events. For the highest excitation energy shown, namely 6 MeV/A (the bottom row of Fig. 8), the dominant feature is the high probability for the symmetric ternary breakup, ≈16.5%, independent of the spin of the system. Apparent for a spin of $0\hbar$ are branches originating from the corner and reaching toward the center of the triangle, a pattern reminiscent of the experimental data. The yield of evaporation-like events relative to the one of symmetric ternary breakup events is, however, higher in the experimental data as compared to SMM calculations. With increasing system spin, the evaporation-like events vanish in favor of the fission-like events. To make an appropriate comparison with the experimental data, we subsequently selected SMM events that populated the central region of the Dalitz diagram ($R_{\rm sym} = 0.08$).

Following the initial qualitative observations of the overall charge correlation patterns produced by SMM as a function of E^*/A and J, more quantitative comparisons with the experimental data were made. Our aim in making these quantitative comparisons is to determine whether a suitable range in E^*/A and J exists that adequately describes the sizes of the three fragments involved in the symmetric ternary breakup. We compare the average sizes of the three fragments as well as the total charge of the three fragments, $Z_{\rm TOT}$, namely $Z_{\rm TOT} = Z_H + Z_M + Z_L$. Displayed in Fig. 9 are the results of SMM calculations (solid lines) as a function of the excitation energy of the system. Different lines for the SMM calculations correspond to different assumed values for the system spin as indicated in the figure. For reference the

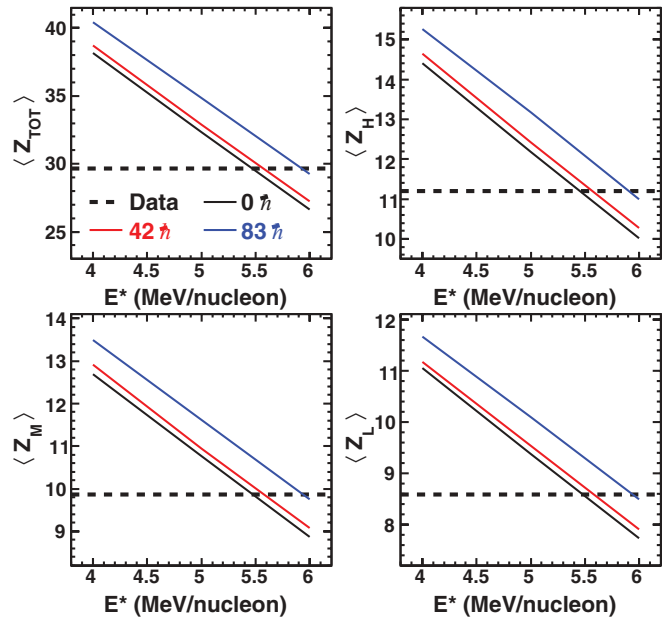

FIG. 9. (Color online) Average sizes for symmetric ternary breakup events as a function of excitation energy. Top left: Average $Z_{\rm TOT}$ (see text for definition) for the experimental data (dashed line) and for the SMM calculation with $J = 0\hbar$ (black solid line), $J = 42\hbar$ (red solid line), and $J = 83\hbar$ (blue solid line). Top right: Average Z_H. Bottom left: Average Z_M. Bottom right: Average Z_L.

experimentally measured values for each quantity are shown as the dashed horizontal line. For a given spin, the average size for all three fragments decreases with increasing excitation energy by ≈30%. While the fragment sizes are very similar for a spin of $0\hbar$ (black solid line) and $42\hbar$ (red line), an extreme spin of $83\hbar$ (blue line) corresponds to an increase of the average Z value between 0.8 and 1. The experimental fragment sizes seem to correspond to an excitation energy of ≈5.5 MeV/A for no or moderate spin, or a slightly higher excitation of ≈6 MeV/A for an extreme spin of $83\hbar$. For systems of similar size and excitation energy [21,40], a spin of $40\hbar$–$50\hbar$ has been deduced. Unfortunately, the experimental acceptance does not permit us to completely reconstruct the PLF* and its spin in the present data set. On the basis of previous work, we judge that for a system size of $A = 103$, a spin of $83\hbar$ is too large [21,40]. We therefore focus on the cases of low and moderate spin, namely $0\hbar$ and $42\hbar$.

Having constrained the events selected by the overall charge correlation pattern, the size of the individual fragments, and the velocity order of the heavy fragment, we next examine the composition of the fragments produced in these projectile fragmentation events. The fragment composition is particularly interesting as there is evidence that the isotopic composition of the fragments produced provides a signal of the density dependence of the nuclear symmetry energy [5]. In previous work however the extraction of the symmetry energy from the decaying PLF* was convoluted with the N/Z equilibration ("isospin diffusion") when the projectile and target are in contact. In contrast, in the present data set the N/Z of the ^{112}Sn target (1.24) and the ^{124}Xe projectile (1.30) are essentially the same, minimizing the impact of the N/Z equilibration stage. Moreover, comparison with data from the ^{124}Sn target (1.48) allows us to assess the impact of the N/Z equilibration.

For the angular range considered, fragments with $Z \leqslant 14$ were isotopically identified. The ratio of the average neutron number to the atomic number, $\langle N\rangle/Z$, is presented in Fig. 10. It is clearly evident that $\langle N\rangle/Z$, predicted by the SMM model

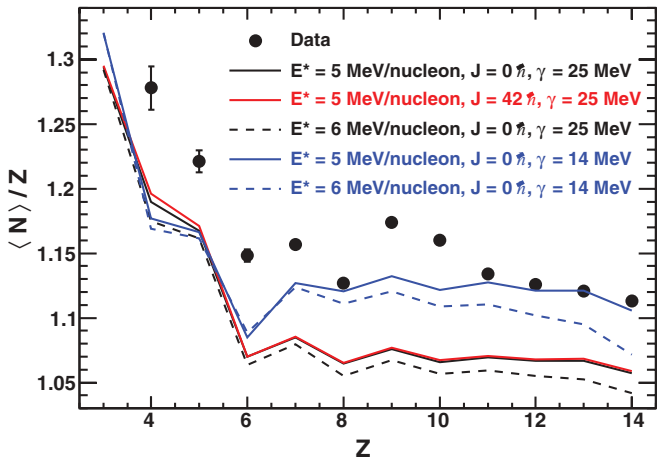

FIG. 10. (Color online) Average N over Z for symmetric ternary events. The solid circles represent the experimental data; the different lines represent the results from SMM calculations as indicated in the figure.

with the standard value of $\gamma = 25$ MeV (black and red lines), is systematically lower for all elements as compared to the experimental data (solid circles). Reduction of the symmetry energy parameter γ from the standard value to a value of 14 MeV (blue lines) raises the average neutron number of the heavy fragments, $Z > 6$, but does little to $\langle N\rangle/Z$ for $Z < 6$. The sensitivity of $\langle N\rangle/Z$ for $Z > 6$ on the symmetry energy parameter emphasizes the importance of measuring the isotopic composition of such heavy fragments.

The normalized isotopic distributions $4 \leqslant Z \leqslant 14$ are shown in Fig. 11 for symmetric ternary events. Solid circles represent the data, and the different lines correspond to different SMM calculations. Depicted in Fig. 11 are the SMM isotopic distributions with $\gamma = 25$ MeV, for an excitation energy of 5 MeV/A with a spin of $0\hbar$ (solid black line) and a spin of $42\hbar$ (solid red line) and for an excitation of 6 MeV/A with no spin (dashed black line). Because of finite experimental resolution, the simulated distributions present more isotopes as compared to the experimental data. For all calculations with the standard value of $\gamma = 25$ MeV, a significant difference exists between the distributions from the model calculation and the experimental ones. The SMM calculations clearly underpredict the yield for neutron-rich isotopes. This deficiency of neutron-rich isotopes increases with increasing Z. In addition, the SMM calculations also predict a significant yield for ^{12}N, ^{14}O, ^{19}Ne, ^{21}Na, ^{25}Al, and ^{27}Si.

The impact of the initial spin, within the model, on the isotope distributions is evident by comparing the isotopic distributions associated at an excitation energy of 5 MeV/A with no spin (solid black line) or moderate spin (solid red line). These distributions are very similar, indicating a very weak dependence of the isotopic composition on the initial spin of the system. As the the excitation energy is increased from 5 to 6 MeV/A, the relative production of neutron-deficient isotopes increases at the expense of that of neutron-rich isotopes. For calculations at excitation energies of 5 and 6 MeV/A, the average neutron multiplicity is essentially unchanged in value, $\langle M_n\rangle = 12.1$. Over this same excitation energy interval, the average proton multiplicity exhibits a slight increase from ≈2.8 to ≈3.1 with increasing excitation energy. Therefore, the free-particle emission, neutrons and protons, cannot be responsible for the change in the fragment isotopic composition. As the excitation energy increases in this range, the average α particle multiplicity increases from ≈1.6 to ≈2.5. For the same range in excitation energy, light neutron-rich cluster multiplicities increase significantly. The average deuteron multiplicity increases from ≈0.95 to ≈1.6, that of tritons from ≈0.6 to ≈1.05, and that of ^{6}He particles from ≈0.06 to ≈0.1. This increased emission of $N > Z$ particles might be responsible for the increased yield of $N = Z - 1$ fragments.

Since a reduced value of the symmetry energy parameter, $\gamma = 14$ MeV for $E^*/A = 5$ MeV, was able to reproduce the behavior of $\langle N\rangle/Z$, as shown in Fig. 10, we examined the impact of reducing γ on the isotope distributions. As γ is reduced, the predicted isotope distributions (represented in Fig. 11 by the blue line) become noticeably broader with significantly increased yield for neutron-rich fragments. Thus

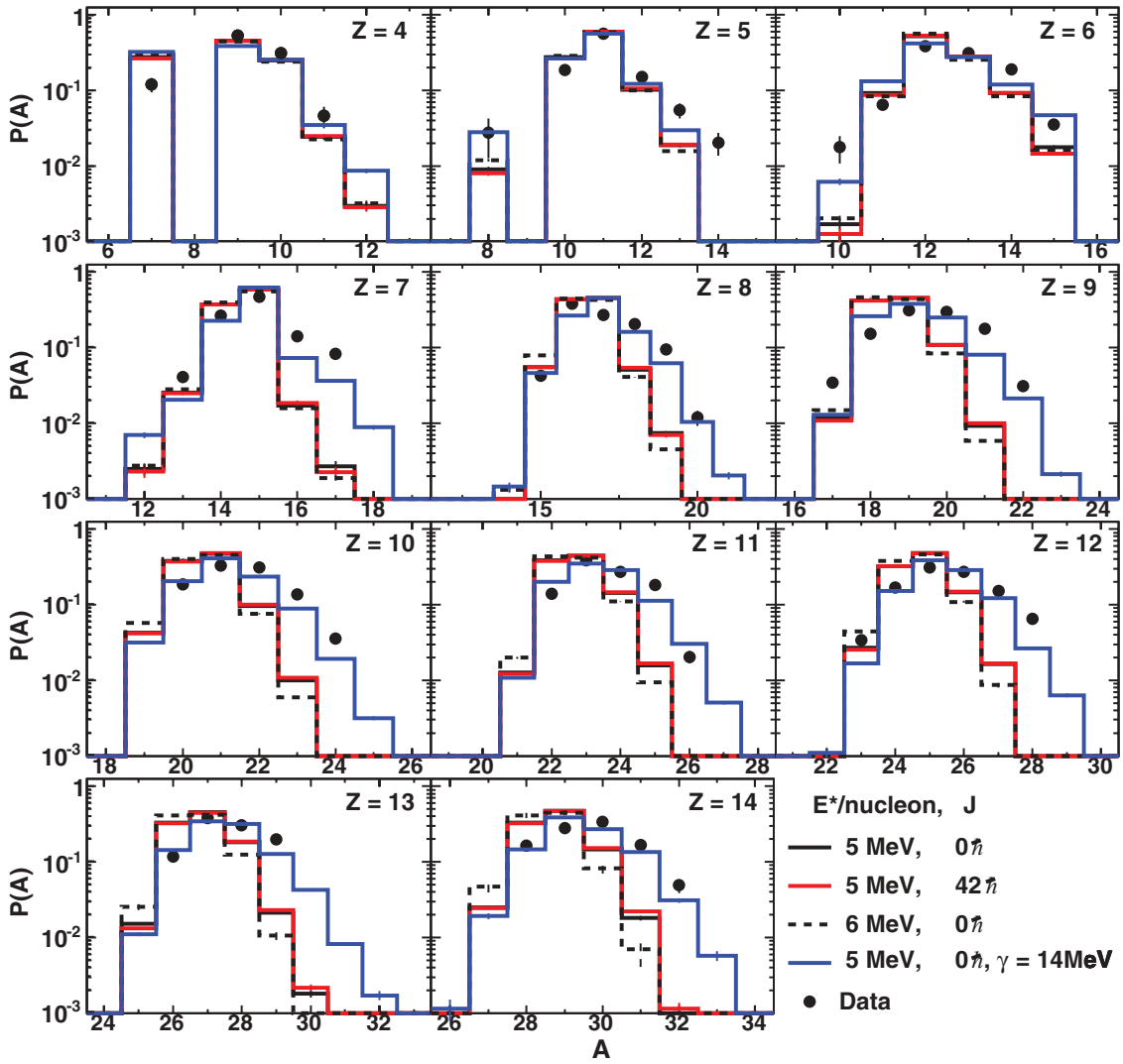

FIG. 11. (Color online) Isotopic distributions for $Z = 4$ to $Z = 14$ for symmetric ternary events. The solid circles represent the experimental data; the different lines represent the results from SMM calculations as indicated in the figure. Error bars shown represent the absolute errors on the relative yield.

the increase in $\langle N \rangle / Z$ that occurs with a reduction in γ is not associated with a shift toward neutron-rich fragments, but a broadening that favors neutron-rich fragments. This behavior can be understood since a reduction in the value of γ corresponds to a reduction in the penalty for creating neutron-rich fragments. For the reduced value of γ shown, one observes reasonable agreement between the experimental isotope distributions and those calculated within SMM. Calculations with a higher excitation energy would require a lower value of γ to reproduce the observed isotope distributions. It is interesting to note that neutron-rich heavy fragments ($Z \geqslant 7$) are particularly sensitive to the value of the symmetry energy parameter. For the standard value of $\gamma = 25$ MeV, SMM underpredicts the yield of neutron-rich heavy fragments in many cases by more than an order of magnitude.

To explore whether this reduction in γ is strictly associated with the statistical ternary breakup of the PLF* or is somehow an artifact of the particular selection criteria we have imposed, we examined the isotope distributions for all ternary events with $Z_L \geqslant 5$. As the asymmetric ternary events are more plentiful by almost an order of magnitude, not selecting on the charge asymmetry is dominated by the asymmetric case. The isotope distributions associated with ternary and symmetric ternary events are compared in the left column of Fig. 12. For fragments with $8 \leqslant Z \leqslant 14$, those most sensitive to the value of γ, the distributions are essentially identical. Clearly the requirement of the symmetric breakup does not dramatically alter the isotope distributions.

We have also examined the isotope distributions associated with ternary PLF* breakup in the reaction $^{124}\mathrm{Xe} + ^{124}\mathrm{Sn}$ at $E/A = 50$ MeV. In the case of this neutron-rich target one might expect that the fragment isotope distributions might reflect the increased neutron content of the initial system. As clearly evident in the right column of Fig. 12, the isotope distributions are very similar. No significant systematic differences are visible. From this similarity one concludes that

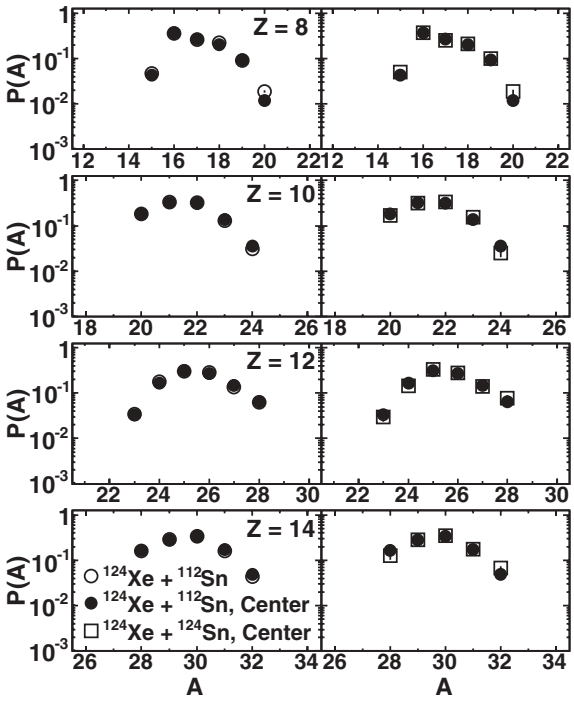

FIG. 12. Experimental isotopic distributions for selected Z for ternary events. The solid (open) circles represent the data for symmetric (all) ternary events for the $^{124}\mathrm{Xe} + ^{112}\mathrm{Sn}$ system. The open squares represent the data for symmetric ternary events for the $^{124}\mathrm{Xe} + ^{124}\mathrm{Sn}$ system. Error bars shown represent the absolute errors on the relative yield.

the additional neutrons present in this neutron-rich target are either not transferred to the projectile during the dynamical stage or are promptly emitted by the PLF* prior to its breakup. The isotope composition of the fragments resulting from ternary decay of the PLF* is not strongly connected to the dynamical stage of the reaction.

V. CONCLUSIONS

Examination of events in which at least three charged particles with $Z \geqslant 2$ are detected in the angular range $3^\circ \leqslant \theta_{\mathrm{lab}} \leqslant 14^\circ$ allows investigation of projectile fragmentation. Inspection of the charge correlation patterns between these three particles reveals different classes of events. The most likely outcome is the survival of a heavy projectile-like fragment in coincidence with two α particles. The requirement that all three particles have $Z \geqslant 5$ changes the observed charge correlation pattern. Although the largest probability corresponds to detection of two medium-size fragments of similar atomic number along with a heavy fragment, a symmetric tripartition is also observed with significant probability. For these symmetric breakups, the average total atomic number is $Z_{\mathrm{TOT}} = 30$, almost 60% of the projectile. The center-of-mass velocity of the three fragments is damped from the projectile velocity by 15%, consistent with a significant excitation of the decaying system. Dynamical decays of the PLF* were further suppressed by requiring that the parallel velocity of the heaviest fragment be less than the center-of-mass parallel velocity of the three fragments.

To understand the nature of the symmetric decay channel, we compared the experimental charge correlation with that predicted by two statistical models. A sequential transition state formalism in which particles are evaporated from a hot nucleus, GEMINI, was unable to reproduce the charge correlations for any suitable set of excitation energy and spin considered. We also compared the experimental data with predictions from a statistical multifragmentation model. This model, in which breakup of a low-density nuclear system in a freeze-out scenario is assumed, was able to reproduce the observed charge correlations.

We therefore compared the experimentally determined $\langle N \rangle / Z$ of fragments associated with the symmetric breakups to the results of the SMM calculations. Describing the $\langle N \rangle / Z$ of heavy fragments ($Z > 6$) within the SMM suggests that a reduction of the symmetry energy parameter from $\gamma =$ 25 to 14 MeV is necessary. Previous measurement of the $\langle N \rangle / Z$ of projectile-like fragments produced in dissipative collisions [41] required a similar reduction of the symmetry energy parameter to describe the experimental data in the multifragmentation regime. In this work, however, we show that isotope distributions of fragments, in particular those with $Z > 6$, provide a more stringent constraint on the nuclear symmetry energy. Within the SMM, the yield of neutron-rich heavy fragments depends sensitively on the symmetry energy parameter. Although the sensitivity of the isotope yields to the symmetry energy parameter had been previously realized for light fragments ($Z \leqslant 7$) [42], the present data show that heavy neutron-rich fragments are particularly sensitive to the symmetry energy. This new result underscores the importance of measuring isotopic yields over a broad range of atomic number and exploring the origin of the different sensitivities with atomic number.

ACKNOWLEDGMENTS

We wish to acknowledge the support of the GANIL staff in providing the high-quality beams that made this experiment possible. We are especially grateful to Y. Georget, B. Jacquot, and V. Morel. This work was supported by the US Department of Energy under Grant No. DEFG02-88ER-40404 (IU). Collaboration members from Université Laval recognize the support of the Natural Sciences and Engineering Research Council of Canada.

[1] J. M. Lattimer and M. Prakash, Science **304**, 536 (2004).
[2] M. A. Famiano *et al.*, Phys. Rev. Lett. **97**, 052701 (2006).
[3] D. V. Shetty, S. J. Yennello, and G. A. Souliotis, Phys. Rev. C **76**, 024606 (2007).

[4] J. M. Lattimer and M. Prakash, Phys. Rep. **442**, 109 (2007).
[5] B.-A. Li, L.-W. Chen, and C. M. Ko, Phys. Rep. **464**, 113 (2008).
[6] A. W. Steiner, Phys. Rev. C **77**, 035805 (2008).
[7] M. B. Tsang, Y. Zhang, P. Danielewicz, M. Famiano, Z. Li, W. G. Lynch, and A. W. Steiner, Phys. Rev. Lett. **102**, 122701 (2009).
[8] D.-H. Wen, B.-A. Li, and P. G. Krastev, Phys. Rev. C **80**, 025801 (2009).
[9] X. RocaMaza and J. Piekarewicz, Phys. Rev. C **78**, 025807 (2008).
[10] L. Trippa, G. Coló, and E. Vigezzi, Phys. Rev. C **77**, 061304(R) (2008).
[11] F. Sammarruca and P. Liu, Phys. Rev. C **79**, 057301 (2009).
[12] B. Davin *et al.*, Phys. Rev. C **65**, 064614 (2002).
[13] F. Bocage *et al.*, Nucl. Phys. **A676**, 391 (2000).
[14] J. Colin *et al.*, Phys. Rev. C **67**, 064603 (2003).
[15] S. Piantelli *et al.*, Phys. Rev. Lett. **88**, 052701 (2002).
[16] T. Paduszynski *et al.*, Nucl. Instrum. Methods A **547**, 464 (2005).
[17] MicronSemiconductor, http://www.micronsemiconductor.co.uk/.
[18] C. Metelko *et al.*, Nucl. Instrum. Methods A **569**, 815 (2006).
[19] B. Davin *et al.*, Nucl. Instrum. Methods A **473**, 302 (2001).
[20] I. Tilquin *et al.*, Nucl. Instrum. Methods A **365**, 446 (1995).
[21] R. Yanez *et al.*, Phys. Rev. C **68**, 011602(R) (2003).
[22] R. H. Dalitz, Phys. Rev. **94**, 1046 (1954).
[23] P. Kreutz *et al.*, Nucl. Phys. **A556**, 672 (1993).
[24] R. J. Charity, Phys. Rev. C **58**, 1073 (1998).
[25] D. Drijard, H. G. Fischer, and T. Nakada, Nucl. Instrum. Methods **225**, 367 (1984).
[26] A. B. McIntosh *et al.* (2009), submitted to Phys. Rev. C.
[27] R. J. Charity *et al.*, Nucl. Phys. **A483**, 371 (1988).
[28] R. J. Charity *et al.*, Phys. Rev. C **63**, 024611 (2001).
[29] R. J. Charity *et al.*, Nucl. Phys. **A476**, 516 (1988).
[30] R. J. Charity *et al.*, Nucl. Phys. **A511**, 59 (1990).
[31] E. Le Gentil *et al.*, Phys. Rev. Lett. **100**, 022701 (2008).
[32] J. P. Bondorf *et al.*, Phys. Rep. **257**, 133 (1995).
[33] A. S. Botvina and I. N. Mishustin, Phys. Rev. C **63**, 061601(R) (2001).
[34] L. G. Sobotka, R. J. Charity, J. Tõke, and W. U. Schröder, Phys. Rev. Lett. **93**, 132702 (2004).
[35] J. Tõke, L. Pienkowski, L. G. Sobotka, M. Houck, and W. U. Schroder, Phys. Rev. C **72**, 031601(R) (2005).
[36] L. G. Sobotka and R. J. Charity, Phys. Rev. C **73**, 014609 (2006).
[37] N. Bohr, Nature (London) **137**, 344 (1936).
[38] A. S. Botvina *et al.*, Nucl. Phys. **A475**, 663 (1987).
[39] N. Buyukcizmeci, R. Ogul, and A. S. Botvina, Eur. Phys. J. A **25**, 57 (2005).
[40] J. C. Steckmeyer *et al.*, Nucl. Phys. **A686**, 537 (2001).
[41] G. A. Souliotis, A.S. Botvina, D. V. Shetty, A. L. Keksis, M. Jandel, M. Veselsky, and S. J. Yennello, Phys. Rev. C **75**, 011601(R) (2007).
[42] J. Iglio *et al.*, Phys. Rev. C **74**, 024605 (2006).